JACS
JOURNAL OF THE AMERICAN CHEMICAL SOCIETY
Article
pubs.acs.org/JACS

Direct Spectroscopic Evidence of Ultrafast Electron Transfer from a Low Band Gap Polymer to CdSe Quantum Dots in Hybrid Photovoltaic Thin Films

Elsa Couderc, Matthew J. Greaney, Richard L. Brutchey,* and Stephen E. Bradforth*

Department of Chemistry and the Center for Energy Nanoscience, University of Southern California, Los Angeles, California 90089, United States

Supporting Information

ABSTRACT: Ultrafast transient absorption spectroscopy is used to study charge transfer dynamics in hybrid films composed of the low band gap polymer PCPDTBT and CdSe quantum dots capped with *tert*-butylthiol ligands. By selectively exciting the polymer, a spectral signature for electrons on the quantum dots appears on ultrafast time scales ($\lesssim$ 65 fs), which indicates ultrafast electron transfer. From this time scale, the coupling between the polymer chains and the quantum dots is estimated to be $J \gtrsim$ 17 meV. The reduced quantum dot acceptors exhibit an unambiguous spectral bleach signature, whose amplitude allows for the first direct calculation of the absolute electron transfer yield in a hybrid solar cell (82 ± 5%). We also show that a limitation of the hybrid system is rapid and measurable geminate recombination due to the small separation of the initial charge pair. The fast recombination is consistent with the internal quantum efficiency of the corresponding solar cell. We therefore have identified and quantified a main loss mechanism in this type of third generation solar cell.

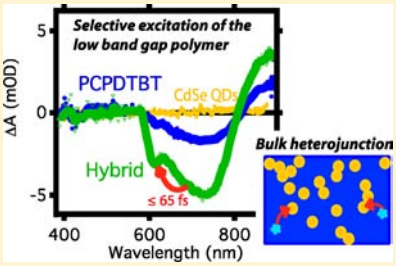

I. INTRODUCTION

Bulk heterojunction (BHJ) hybrid solar cells comprised of semiconductor nanocrystals blended with conjugated polymers are demonstrating improved photovoltaic device performance (up to η_P = 4−5%) over the past 12 years.[1−3] Semiconductor nanocrystals offer spectral tunability through compositional and quantum confinement effects, high dielectric constants, and high electron mobilities when compared to commonly used fullerene acceptors; however, hybrid device efficiencies currently lag behind those of all-organic heterojunctions. Design rationale specific to hybrid systems are being developed to further enhance the efficiencies of these solar cells,[2,4] but the physical mechanisms that occur at the hybrid interfaces are still poorly understood—in particular the formation and evolution of charge transfer states and of mobile charge carriers. While many studies of conjugated polymers and fullerene derivative blends have resulted in the detection of interfacial charge-transfer (ICT) states[5] (e.g., through emission below the band gap of the donor[6] or through new photoinduced absorption (PIA) bands in transient absorption (TA) measurements[7]), possible spectral signatures for such ICT states in hybrid blends have been more elusive.[8−10] A dominant issue in hybrids is the electronic coupling between the nanocrystals, their ligands, and the polymer chains, which is poorly understood yet frequently considered to be responsible for the lower efficiencies of hybrid devices[11,12] when compared to all-organic solar cells. Consequently, direct measurement of the charge transfer processes in hybrid blends is of particular interest. It has heretofore been difficult, however, to disentangle the spectral signatures of all the transient species at play; as a result, measuring how fast these transient species form and decay and/or determining the absolute yield of charge carrier formation has remained a challenge. In most BHJs, the charge transfer yields are evaluated from the contribution of the excited species residing on the polymer because the spectral signature of the acceptor anion is only poorly resolved.[13,14] Despite the spectroscopic signatures of transient species on the acceptor phase in hybrid BHJs,[15−17] the question of charge transfer yield is still largely unanswered.[12,14,18] Furthermore, ultrafast spectroscopy studies have focused on hybrid heterojunctions giving relatively poor photovoltaic efficiencies as a result of long, insulating ligands on the nanocrystal acceptor,[12,19] or reduced absorption of one of the hybrid components (i.e., either wide band gap nanocrystal acceptors[15,16,20] or donor polymer[17]).

Herein, we characterize the electron transfer dynamics and electron transfer yield in a hybrid BHJ blend that (i) demonstrates high power conversion efficiency,[21] as a result of ligand engineering,[2,4] and (ii) allows for clear elucidation of the electron transfer rate and yield because the donor and acceptor phases can be spectrally resolved. The BHJ blends of poly[2,6-(4,4-bis(2-ethylhexyl)-4*H*-cyclopenta[2,1-*b*;3,4-*b*′]-dithiophene)-*alt*-4,7-(2,1,3-benzothiadiazole)] (PCPDTBT, $E_g^{opt} \approx$ 1.5 eV) with *tert*-butylthiol (tBT)-capped CdSe quantum dots, or CdSe(tBT) QDs, give a power conversion efficiency of 2.1%. To study the excited state dynamics, we used spectrally resolved TA spectroscopy with a time resolution of 65 fs. In such an experiment, the sample is excited by an

Received: July 5, 2013
Published: November 7, 2013

dx.doi.org/10.1021/ja406884h | *J. Am. Chem. Soc.* 2013, 135, 18418−18426

ultrafast laser pulse (pump), and its absorption spectrum is measured at a time delay Δt after the pump by a broadband laser pulse (probe). Spectra presented in this paper are given as differences between the steady-state absorption (pump off) and the excited state absorption (pump on) of the sample. The TA spectra therefore explicitly show the depletion of ground state-based transitions and the appearance of excited state transitions. We designed the hybrid system and TA experiment to minimize the number of physical processes occurring at the donor/acceptor interfaces, therefore allowing for straightforward extraction of physical parameters. In particular, when the PCPDTBT is selectively photoexcited, due to the relative alignment of the energy levels of the donor and acceptor, polymer excitons may only dissociate through electron transfer into the QD conduction band. Consequently, this work reveals an unambiguous spectral signature for the QD anion, providing evidence of electron transfer from a donor polymer to a semiconductor nanocrystal acceptor, which occurs within 65 fs for this system. The spectral evidence of excited state species on the acceptor phase is unique to hybrids and allows the electron transfer yield (82 ± 5%) to be determined and the evolution of the electron population on the QDs to be tracked. Finally, rapid geminate recombination is identified and quantified as the main loss mechanism in the corresponding solar cell.

II. EXPERIMENTAL SECTION

Sample Preparation. CdSe quantum dot synthesis and tBT ligand exchange were performed as described in ref 4. PCPDTBT was used as received from 1-Material, with a molecular weight and a polydispersity index of 28.5 kDa and 1.9, respectively. Photovoltaic devices were fabricated and tested in air as described in ref 2 and in the Supporting Information. Device active areas were 4 mm^2, and active layers were ~45−55 nm thick. For spectroscopic studies, hybrid active layers were deposited through a similar spin-casting procedure onto quartz slides. Their thicknesses were adjusted to obtain similar optical densities at 800 nm (i.e., neat PCPDTBT, 15−20 nm; hybrids, 45−55 nm).

Steady-State Spectroscopies. Thin film absolute absorbances were measured using an integrating sphere. Chopped and filtered monochromatic light (250 Hz, 10 nm fwhm) from a Cornerstone 260 1/4 m double grating monochromator (Newport 74125) was used in conjunction with an EG&G 7220 lock-in amplifier to perform spectral responsivity (or EQE) measurements. Thin film photoluminescence spectra were collected on a Horiba Jobin Yvon Nanolog spectrofluorometer equipped with a 450W xenon short-arc excitation source and an IGA-020 InGaAs photodiode detector using 0.5 s integrating time and 3 scan averages, and then they were corrected for the InGaAs detector response function. The photoluminescence intensity is normalized by the absorbance of the film at 780 nm to account for slight differences in film thicknesses.

Femtosecond Transient Absorption (TA) Spectroscopy. TA measurements were carried out using the output of a Coherent Legend Ti:sapphire amplifier (1 kHz, 3.5 mJ, 35 fs), as described in detail elsewhere.[22,23] The amplifier output was used as the 800 nm pump pulse. White light supercontinuum probe pulses were polarized perpendicular to the pump pulse and generated using a rotating CaF_2 window or a sapphire window depending on the probed wavelength range (see Supporting Information). The probe pulse was dispersed by an Oriel MS1271 spectrograph onto a 256 pixel Si or InGaAs photodiode array depending on the wavelength range probed. To obtain satisfactory signal-to-noise on the optically thin samples, transient spectra were measured for typical pump fluences of 180 μJ cm^{-2}. Samples were translated perpendicular to the path of the pump and probe to prevent photodamage.

III. RESULTS AND DISCUSSION

1. Steady-State Characterization of the Hybrid Blends. We investigated BHJs of 4.5-nm CdSe(tBT) QDs with the low band gap conjugated polymer PCPDTBT.[24] The extended absorption profile of PCPDTBT (i.e., absorption cutoff at ~850 nm) coupled with the effects of the tBT ligands on the electronic coupling between QDs[25] result in an efficient BHJ solar cell. Figure 1 shows the absorption spectra of films of

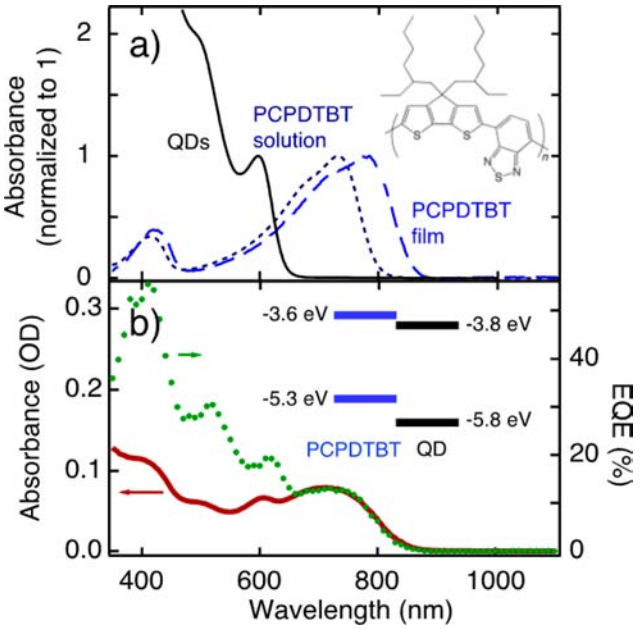

Figure 1. (a) Normalized absolute absorbance spectra of a CdSe(tBT) QDs solution (solid line), a neat PCPDTBT film (dashed line), and a PCPDTBT solution (dotted line). The inset shows the structure of the donor polymer, PCPDTBT. (b) Absolute absorbance of a PCPDTBT:CdSe(tBT) hybrid film with 1:8 wt/wt polymer/QD spin-cast from 1,2-dichlorobenzene onto quartz, and external quantum efficiency of the corresponding ITO/PEDOT:PSS/PCPDTBT:CdSe-(tBT)/ZnO/Al device. The inset shows the energy diagram of the BHJ relative to vacuum, with energy levels of PCPDTBT[24] and of 4.5 nm CdSe(tBT) QDs,[4] all determined from electrochemistry measurements.

PCPDTBT, CdSe(tBT) QDs, and the resulting hybrid BHJ. The 4.5-nm CdSe(tBT) QDs ($E_g \approx 2.1$ eV) exhibit excitonic transitions at 600 nm (overlapping $1S_e-1S_{3/2}$ and $1S_e-2S_{3/2}$ transitions) and 500 nm ($1P_e-1P_{3/2}$ transition).[26,27] A change in the polymer morphology in the presence of the QDs is evidenced by a blue shift of the PCPDTBT peak absorbance relative to that of the neat polymer film (also see the Supporting Information, Figure S1), resulting from the QDs inhibiting packing of polymer chains and/or from the cosolvent required during processing of the hybrid BHJ films.[28]

The external quantum efficiency (EQE) provides evidence for dissociation of excitons generated on both the donor and acceptor phases (Figure 1b). This is evidenced in the EQE spectrum by cooperative spectral response from both the nanocrystals (e.g., excitonic features at 500 and 600 nm) and the polymer at energies lower than the band gap of the QDs (e.g., 750 nm). The corresponding PCPDTBT:CdSe(tBT) QD BHJ hybrid solar cell gives a short circuit current of J_{SC} = 7.25 mA cm^{-2}, an open circuit potential of V_{OC} = 0.76 V, and a fill factor (FF) of 0.38, leading to a power conversion efficiency of

dx.doi.org/10.1021/ja406884h | J. Am. Chem. Soc. 2013, 135, 18418−18426

η_P = 2.1% for a ITO/PEDOT:PSS/PCPDTBT:CdSe(tBT)/ZnO/Al device structure (see the Supporting Information, Figure S2). The active layer of this device is the same as that studied by TA spectroscopy (*vide infra*). Efficiencies of 4.1% have been achieved for this system by substituting the CdSe QDs with anisotropic CdSe multipods.[2]

In order to understand how the two components of the hybrid heterojunction give rise to photocurrent upon photoexcitation, we performed both steady-state and time-resolved spectroscopic measurements. Photoluminescence tracks the excited state population and dynamics. The presence of CdSe(tBT) QDs in a PCPDTBT matrix results in the reduction of the polymer photoluminescence and is an indication of the interaction between the two components. Photoluminescence quenching experiments (Figure 2) illustrate

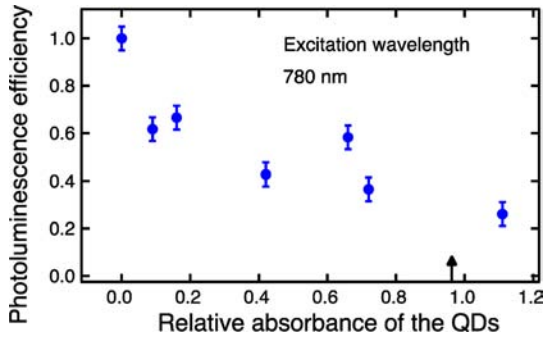

Figure 2. Photoluminescence efficiency as a function of the QD content in the hybrid, for an excitation wavelength of 780 nm. The quantum dot content was evaluated from the ratio of the absorbance at the wavelength at which the polymer absorbs least (at 480 nm the absorbance is mainly due to QDs) and of the absorbance at the wavelength at which the polymer absorbs most (714–774 nm depending on the film). The photoluminescence efficiency was determined by integrating the absorbance-corrected PL signals of each film from 850 to 1100 nm. The relative absorbance of the sample presented in the transient absorption section is shown by a black arrow.

that the addition of CdSe(tBT) QDs reduces the photoluminescence efficiency of PCPDTBT by as much as 75 ± 5% for the maximal QD content studied here (1:10 wt/wt polymer/QD). To understand the type of interaction that results in photoluminescence quenching, it is important to note that the respective band gaps of the components prevent uphill energy transfer from the polymer to the QDs (inset of Figure 1b). Furthermore, while the modifications of the polymer packing detected by absorbance measurements can affect the photoluminescence efficiency by altering radiative and nonradiative decay pathways, we would expect that the more disordered, glassy phase of PCPDTBT observed in the hybrid films would be more emissive than the more ordered phase in neat PCPDTBT films, as observed in P3HT.[29] Consequently, the photoluminescence quenching experiments suggest that charge transfer does indeed occur at the interface between the PCPDTBT and the CdSe(tBT) QDs, as confirmed by the experimental evidence presented below.

2. Transient Absorption Spectra of Hybrid Components. TA measurements were performed to directly quantify the charge-transfer processes at play in the hybrid blend. The low band gap polymer was selectively excited by pumping the films at 800 nm, which is in the low-energy tail of the $S_1 \leftarrow S_0$ transition of PCPDTBT.[30] First, we established that all measurements were performed in the linear regime, as determined by probing the initial singlet population in neat PCPDTBT films for a range of pump fluence (Figure 3a). The

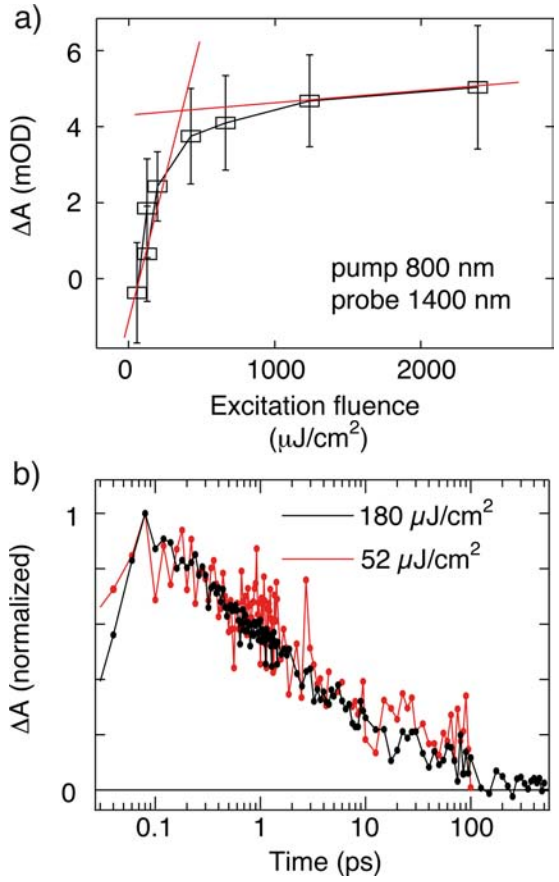

Figure 3. (a) Transient absorption signal amplitude of a neat PCPDTBT film at 1400 nm, taken at 1 ps delay after the pump pulse. (b) Time-resolved transient absorption signal for a PCPDTBT:CdSe(tBT) QD hybrid film probed at 1400 nm (singlet exciton, see text) after excitation by a 800 nm pump pulse for two different pump fluences.

inflection of the curve at around 250 μJ cm^{-2} (corresponding to 1.4 × 10^{14} absorbed 800 nm photons per cm^2) shows the threshold above which exciton–exciton and exciton–charge annihilation effects become non-negligible. The threshold fluence 250 μJ cm^{-2} corresponds to a number density ρ_c of absorbed photons of 9 × 10^{-2} nm^{-3} in a 15 nm film. The pump fluence used for the production run TA experiments was set at 180 μJ cm^{-2} for the 800 nm and for the 550 nm pumps. We further checked that this pump fluence indeed corresponds to the annihilation-free regime in hybrid films by recording the time-resolved exciton decay for different fluences. Figure 3b shows that the exciton decays are comparable for fluences of 180 μJ cm^{-2} and 52 μJ cm^{-2}, indicating the absence of nonlinear processes at these pump fluences.

Now spectral features for neat CdSe(tBT) QD, neat PCPDTBT polymer, and hybrid films are compared in Figure 4 for different time delays between the pump and the probe. The dynamics of the different excited state populations are extracted and summarized in Figure 5. The TA data have been normalized by the excitation densities in each sample to eliminate the slight differences in absorbance of the neat component films and of the hybrid films due to thickness and

dx.doi.org/10.1021/ja406884h | J. Am. Chem. Soc. 2013, 135, 18418–18426

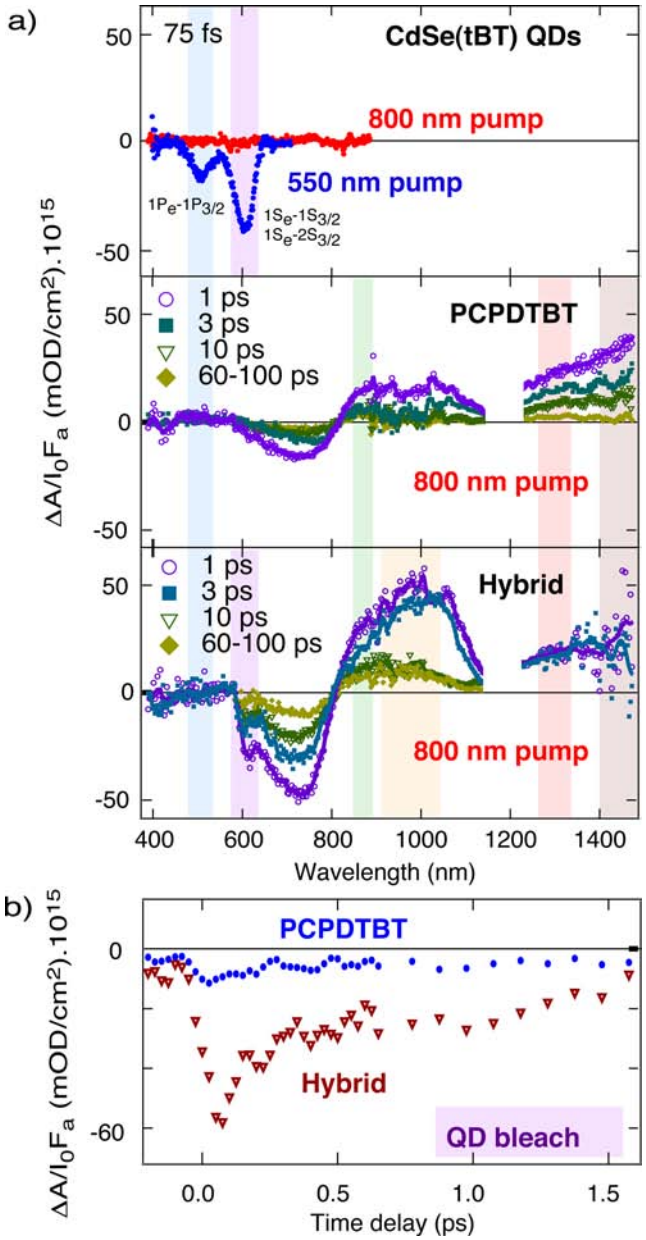

Figure 4. (a) Transient absorption spectra of a neat CdSe(tBT) film, of a neat PCPDTBT film (15−20 nm), and of a hybrid PCPDTBT:CdSe(tBT) film (1:8 wt/wt, 45−55 nm) at different time delays between the pump and the probe pulses. I_0 is the incident pump photon density ($I_0 \sim 7.3 \times 10^{14}$ cm^{-2} for the 800 nm pump; 5×10^{14} cm^{-2} for the 550 nm pump), while F_a is the fraction of 800 nm photons absorbed by the films ($F_a \sim 0.14$ for both the polymer and the QD films, $F_a \sim 0.09$ for the hybrid). We identify the spectral features discussed in the text by color-coding. (b) Open symbols show the QD bleach formation (600−620 nm, violet shading) within the time resolution of the setup. The small signal in the trace from the neat polymer film, full symbols, is due to the overlapping polymer ground state bleach.

morphology differences; the raw data (signals in mOD) is shown in Figure S3 for completeness (see the Supporting Information). Here, the spectra of the neat CdSe(tBT) QD film and the spectra of the neat PCPDTBT film serve as control experiments to disentangle transient species present in the hybrid data.

First, Figure 4a shows the absence of signal from the neat CdSe(tBT) QD film when it is excited at 800 nm, ruling out two-photon absorption and/or trap-state absorption as possible QD excitation pathways at this excitation wavelength. This stands in contrast to transient spectra obtained when a 550 nm pump is used that directly excites the CdSe(tBT) QD film. The latter experiment reveals bleaches of the overlapping $1S_e-1S_{3/2}$ and $1S_e-2S_{3/2}$ transitions of the QDs around 610 nm and of the $1P_e-1P_{3/2}$ transition around 500 nm.[26,27]

Second, PCPDTBT singlet excitons can be monitored directly in the near-infrared (NIR) region through the induced absorption band around 1400−1480 nm (brown shading in Figure 4a), which is attributed to transitions from the lowest lying singlet excited state to higher lying singlet states ($S_n \leftarrow S_1$).[31] The 1250 nm PIA signal of neat PCPDTBT (red shading in Figure 4a) has been previously associated with dissociated/delocalized polarons[31,32] (labeled "polarons I"). This signal overlaps with the broad singlet exciton PIA around 1400 nm, but the polarons I band can be detected at long times ($\gtrsim$100 ps) when the singlet band disappears.[31] The positive feature in the 855−885 nm range (green shading) has also been observed in absorption spectra of chemically oxidized PCPDTBT[33,34] and is therefore also attributed to polarons. In our TA measurements, this feature shows a significant long-lived component (lifetime >500 ps, Figure 5) that distinguishes it from the polaron I band. It is therefore likely related to a different polaron species, labeled "polarons II". Polarons II may correspond to trapped/localized polarons,[35,36] possibly caused by morphological defects.

3. Transient Absorption Spectra of Hybrid Films. For hybrid films, the TA measurements provide clear evidence that electron transfer occurs from PCPDTBT to the CdSe(tBT) QDs upon excitation at 800 nm. The hybrid film exhibits an additional negative peak around 610 nm when compared to the neat polymer film (violet shading in Figure 4a). This peak corresponds to a bleach of the CdSe(tBT) QD $1S_e-1S_{3/2}$ and $1S_e-2S_{3/2}$ excitonic transitions (Figure 1a and Figure 4a). As noted before, and as shown on the inset of Figure 1b, this signal can only arise from electron transfer from the excited polymer to the QDs; both energy transfer from the exciton state of PCPDTBT to the exciton state of CdSe(tBT) QDs and hole transfer from PCPDTBT to the QDs are uphill processes. Moreover, the 610 nm bleach arises very rapidly within the time resolution of our ultrafast measurement, namely 65 fs (Figure 4b and see the Supporting Information).

In the 900−1050 nm (orange shaded) region, the hybrid films exhibit a long-lived component that is fully absent in the neat polymer. This long-lived PIA is therefore related to the presence of QDs in the blend. It could arise from electronic transitions in the reduced CdSe(tBT) QDs[37,38] after charge transfer or from transitions from states akin to CT states that involve positive polarons on the polymer chains and electrons on the QDs. Although there is a small signal in this 900−1050 nm region in the neat polymer films, its decay dynamics are similar to that of the singlet and polarons bands (see the Supporting Information, Figure S5). Therefore, this neat polymer film signal can be distinguished from the large and long-lived signal observed in the hybrid films in the orange shaded region. In addition, both the prompt polymer bleach (observed at 600−800 nm) and the prompt polaron II signal (green shading) are enhanced in the hybrid, suggesting a higher yield of charge carriers by a factor 2−3 at 1 ps, comparable to the yield enhancement in PDTPQx-HD:PbS hybrid hetero-

dx.doi.org/10.1021/ja406884h | J. Am. Chem. Soc. 2013, 135, 18418−18426

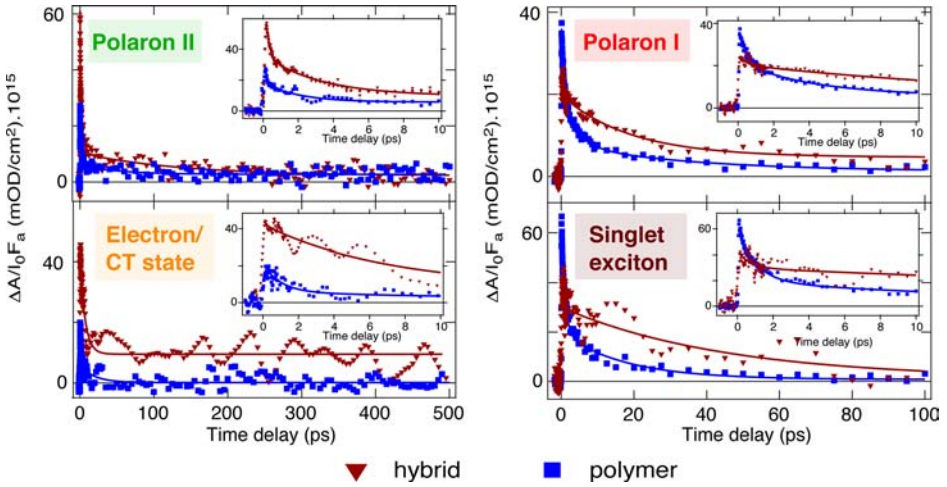

Figure 5. Comparison of the decay dynamics of the excited species in the neat PCPDTBT film (squares, blue symbols) and in the hybrid film (triangles, brown symbols), with short time dynamics given as insets. Time traces were obtained by averaging data over the following wavelength ranges: green 855−885 nm, orange 900−1050 nm, red 1250−1300 nm, brown 1400−1480 nm. The full lines are multiexponential fits to the data to serve as guides to the eyes; their coefficients can be found in Table S1 of the Supporting Information. The data point traces for the hybrid samples in the orange, red, and brown wavelength ranges were smoothed by 5 points boxcar averaging.

junctions determined by steady-state PIA.[39] Finally, the PCPDTBT singlet exciton $S_n \leftarrow S_1$ transition(s) amplitude is partially quenched by ∼33% at initial times (75 fs) in the hybrid, as compared to the neat polymer film (Figure 5). This can result from (i) a reduction of the initial S_1 exciton population caused by electron transfer to the QDs, and/or (ii) a modified oscillator strength of the $S_n \leftarrow S_1$ transitions caused by packing modifications of the polymer, and/or (iii) overlapping bands from various excited species.

4. Accessible QD Electron Energy Levels by Injection from the PCPDTBT S_1 State. The TA experiments presented in this paper lead to a clearer understanding of the electronic couplings at play in the PCPDTBT:CdSe(tBT) QD hybrid system. First, the spectral information given by the TA data set helps discriminate between filled electron levels in the CdSe(tBT) QDs. The bleached $1S_e-1S_{3/2}$ and $1S_e-2S_{3/2}$ transitions indicate that the $1S_e$ level of the QD is partly filled upon electron transfer from the polymer donor. On the other hand, due to the spectral overlap in the 500 nm region with a singlet state absorption of the polymer (blue shading in Figure 4; also see the Supporting Information, Figure S6), it is difficult to confirm filling of the $1P_e$ electron level from TA experiments; however, the energy level alignment (Figure 1b) gives information on the filling of the $1P_e$ level. In CdSe QDs, most of the energy difference between the first $(1S_e-1S_{h,1/2})$ and second $(1P_e-1P_{h,1/2})$ excitonic transitions derives from the energy level difference in the conduction band due to the near degeneracy of the valence band.[40] This excitonic transition energy difference is on the order of 400 meV for the 4.5 nm CdSe QDs used here, which implies that the $1P_e$ level of the 4.5 nm CdSe(tBT) QD probably lies shallower in energy than the ionization potential of the PCPDTBT excited state, $IP^*_{PCPDTBT}$ (*vide infra*). Therefore, it is likely that electron transfer from PCPDTBT excited at 800 nm to the $1P_e$ level of CdSe QDs is energetically unfavorable.

5. Evaluation of the Electronic Coupling between PCPDTBT and CdSe(tBT) QDs. The ultrafast electron transfer time $t_{et} \lesssim 65$ fs ($k_{et} \gtrsim 1.5 \times 10^{13}$ s^{-1}) shows that the PCPDTBT S_1 excited state and the QDs $1S_e$ electron state are well coupled. Under the assumption of a three-level scheme[41] (i.e., ground state, polymer excited state, and electron-transferred state), the electronic coupling J between the S_1 excitonic state of PCPDTBT and that of the CdSe(tBT) QDs can be evaluated from Marcus theory: $k_{et} = (t_{et})^{-1} = 2\pi J^2/\hbar(4\pi\lambda k_B T)^{1/2} \exp(-(\Delta G + \lambda)^2/4\lambda k_B T)$, where J is the electronic coupling matrix element, $\hbar$ is the reduced Planck constant, λ is the reorganization energy, k_B is the Boltzmann constant, T is the temperature, and ΔG is the driving force for the electron transfer reaction. The driving force ΔG cannot directly be inferred from the electron affinities measured by electrochemistry and pictured in Figure 1b because this would neglect the exciton binding energy. We therefore use[42] $\Delta G \sim EA_{QD} - IP^*_{PCPDTBT}$, where EA_{QD} is the adiabatic electron affinity of the QD and $IP^*_{PCPDTBT}$ is the adiabatic ionization potential of the excited PCPDTBT donor. Approximating $IP^*_{PCPDTBT}$ as $IP_{PCPDTBT} - E_{exciton}$, and with the electrochemically determined energy levels for $IP_{PCPDTBT}$ and EA_{QD}, we find $\Delta G \sim -100$ meV. The reorganization energies for charge transfer from a conjugated polymer to a QD are poorly documented at this stage, but the minimal value of the electronic coupling J can be obtained using the optimal reorganization energy value (i.e., such that $\lambda + \Delta G \sim 0$ meV), which yields $J \gtrsim 17$ meV. This value is comparable to the optimal coupling matrix element obtained for electron transfer from PbS QDs to PCBM molecules derived with the same hypothesis.[12] The measured electron transfer time is also consistent with the measured electron injection times in dye-sensitized solar cells[43] and with calculated electron injection times of 90 fs from dodecathiophene chains physisorbed to Si nanocrystals.[44] To date, no signature of an optically bright CT state has been unambiguously detected in this hybrid system, supporting the assumption of a three-level scheme.

Although electron transfer from the S_1 state of PCPDTBT and the $1S_e$ state of CdSe QDs is "ultrafast" in our hybrid system (i.e., below the 65 fs resolution of our setup), it does not directly imply that it always outcompetes all other processes, leading to 100% of the excitons dissociated at donor/acceptor interfaces, as is commonly assumed.[45,46] Indeed, in highly disordered materials such as hybrid and organic BHJs, the interface is a heterogeneous ensemble that exists as a

dx.doi.org/10.1021/ja406884h | J. Am. Chem. Soc. 2013, 135, 18418−18426

distribution of donor−acceptor conformations and couplings. Moreover, the distribution of couplings is likely widened in hybrid materials compared to PCBM-based BHJs as a result of the intrinsically heterogeneous nature of QD surfaces (i.e., variety of crystalline facets, ligand configurations, and polydispersity of QD diameters). In these experiments, we therefore likely observe a subset of donor/acceptor interface conformations, namely those exhibiting the strongest couplings. It is possible that additional, slower electron transfer processes take place and that these slower charge separation events are hidden by the fast decay of the rapidly charge-transferred pairs. Disorder, *via* the most unfavorable conformations, or equivalently the slowest electron transfer processes, can reduce the absolute yield of charge transfer below 100%.

6. Prompt Yield for Electron Transfer and Model for the Electron Population Time Evolution. The QD spectral bleach provides a way to quantify the absolute yield of charge transfer at the donor/acceptor interface. This task is generally difficult in all-organic BHJs because the numerous PIA signatures of excited states in the NIR overlap strongly, making quantitative analysis difficult. Here, the 610 nm signal arises from CdSe(tBT) QD reduction only, so that its amplitude reflects the number of electrons located on the QD at each delay time of the TA experiment. In order to eliminate the polymer bleach contribution in this region, the hybrid TA spectra can be decomposed at each time by a linear combination of the CdSe(tBT) QD and of the neat PCPDTBT TA spectra. For each time step, the observed data d_{obs} (corresponding to the hybrid spectrum) can be compared to the data d_{pred} predicted by a linear combination model with parameters (a,b):

$$d_{obs} = \Delta A_{hybrid}$$
$$d_{pred} = a \times \Delta A_{polymer} + b \times \Delta A_{QD}(t = 75\ \text{fs}) \quad (1)$$

where ΔA_i is the TA signal of sample i (Figure 4a). The comparison between d_{obs} and d_{pred} is made for a large number of (a,b) parameter couples. The most likely model parameter couple (a_{mean}, b_{mean}) is extracted using Bayes' theorem and a Metropolis algorithm.[47] It is possible to fit the data, within experimental uncertainties, with various (a,b) couples; therefore, the standard deviations of the parameters $(a_{s.d}, b_{s.d.})$ reflect the dispersion of (a,b) couples that fit the experimental data. Simply put, this procedure gives access to rigorous, statistically relevant error bars (see the Supporting Information).

In this decomposition, the parameter b represents the contribution of the QD electrons to the hybrid spectrum. The parameter b can be converted to the density of electrons, N_e, residing on the QDs:

$$N_e = b \times I_{0,QDs} \times F_{a,neatQD} \times F_{1Se} \quad (2)$$

where $I_{0,QDs}$, $F_{a,neatQD}$, and F_{1Se} are the experimental parameters used for the control experiment on the neat QD film: $I_{0,QDs} \sim 5 \times 10^{14}$ cm^{-2} is the density of 550 nm photons incident on the neat QD film, $F_{a,neat\ QD} \sim 0.14$ is the fraction of 550 nm photons absorbed by the neat QD film, and $F_{1Se} \sim 0.68$ is the fraction of absorbed photons involving the $1S_e$ state of the QD conduction band (see the Supporting Information). In other words, the 610 nm bleach magnitude in the neat QD film, obtained after the generation of $I_{0,QDs} \times F_{a,neatQD} \times F_{1Se} \sim 5 \times 10^{13}$ cm^{-2} electrons on the $1S_e$ energy level is used to deduce the density of electrons on the QDs in the hybrid film from the 610 nm bleach magnitude.

The population density of electrons on the conduction band of the QDs as a function of time is represented in Figure 6.

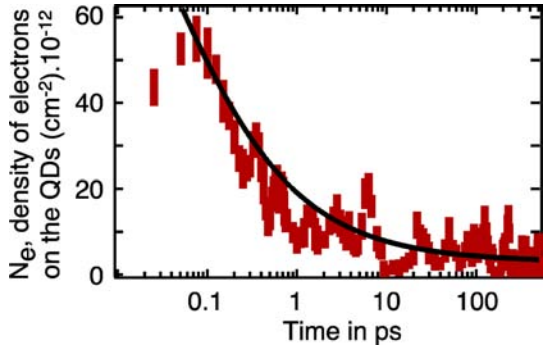

Figure 6. Density of electrons located on the QD conduction band as a function of time. This curve is obtained from the deconvolution of the 610 nm TA bleach, with corresponding statistical error bars (brown bars). A solution to the electron−hole pair diffusion problem, under mutual Coulomb attraction, is shown with the black line and described in the text.

Overall, our deconvolution model assumes that (i) each absorbed photon yields one electron−hole pair in a neat QD film or one polymer exciton in a hybrid film, (ii) an extra electron on a QD results in the same magnitude of bleach (in mOD) as an optically excited electron−hole pair,[48] and (iii) the transient spectra measured in the hybrid films can be fitted by a linear combination of the TA spectra measured in the neat QD film and in the neat polymer film in the bleach region (i.e., the amplitude of the PIA features in the spectra of the hybrid are proportional to the PIA features in the neat component films).

Having gained access to the QD electron density as a function of time, we now (i) deduce the prompt yield of electron transfer and (ii) analyze the temporal evolution of the QD electron density with a physically relevant model that describes diffusion of electron−hole pairs, taking account of their mutual Coulomb attraction. Thereby, we avoid the more commonly used (but less physical) fit to multiexponential decays.

i. Prompt Yield of Electron Transfer. The yield of electron transfer is obtained by normalizing the initial electron density (i.e., the electron density extracted at 75 fs) by the exciton density initially present on the PCPDTBT chains: $\eta_{CT} \sim N_e/(I_0F_a)$, where $I_0 \sim 7.3 \times 10^{14}$ cm^{-2} is the density of 800 nm photons incident on the hybrid film, $F_a \sim 0.09$ is the fraction of photons absorbed by the hybrid film. We obtain $\eta_{CT} \sim 82 \pm 5\%$. This number is in general agreement with the charge transfer yield obtained from photoluminescence data.

ii. Temporal Evolution of the QD Electron Density. The QD electron density exhibits a rapid temporal decay that we attribute to recombination with the PCPDTBT polarons. Indeed, the decay observed in the PCPDTBT:CdSe(tBT) QDs hybrids is greatly accelerated compared to the decay observed in neat films of CdSe QDs (the decays are compared in the Supporting Information, Figure S7). This observation rules out the hypothesis that the rapid dynamics observed in hybrids are related to localized excited states (traps) that exist at the surface of the QDs, which would result in longer ground state bleach recovery. We further assume that the blending with the polymer does not introduce localized electron states at the QD surface.

A simple physical model for the recombination of CdSe(tBT) QD electrons and PCPDTBT polarons is that of charges diffusing under a spherically symmetric potential U:[49]

$$\frac{\partial \rho}{\partial t} = \vec{\nabla} \cdot D\left(\vec{\nabla}\rho + \frac{\rho}{k_B T}\vec{\nabla}U(\vec{r})\right) + \delta(\vec{r} - \vec{r_0})\,\delta(t - t_0) \quad (3)$$

where ρ is the density of charges. $U(\vec{r}) = k_B T(r_c/|\vec{r}|) + \vec{E}\cdot\vec{r}$ is the potential, where the first term represents the Coulomb attraction between charges *via* the Onsager radius $r_c = e^2/4\pi\varepsilon_0\varepsilon_r k_B T$ and where the second term is the potential from an external electric field $\vec{E}$. D is the diffusion coefficient and is homogeneous in our case, with $D = (k_B T)/q(\mu_e + \mu_n)$. In this model, recombination between QD electrons and PCPDTBT polarons is geminate. In effect, the decay of the electron population in the hybrid film does not depend on the fluence (see the Supporting Information, Figure S8), providing evidence for geminate recombination. If bimolecular recombination dominated, the electron population decay would be slower for lower pump fluences.

The solution of this equation in the long-time limit is the Braun–Onsager model,[50,51] commonly used to describe the dynamics of charge carrier population at longer time scales.[45,52] Here, the external electric field $\vec{E}$ is null (to match the conditions of the TA experiment), and the force felt by the charges is solely from their Coulomb attraction. We use a differential equation solver[53] to obtain the *time-dependent* solution of eq 3 (i.e., the electron density as a function of time). The specific solution presented in black in Figure 6 has been obtained for a diffusion coefficient $D = 5 \times 10^{-5}$ cm^2 s^{-1}, calculated from measured mobility values for electrons and holes in hybrid blends made of P3HT and CdSe QDs.[28] We find that diffusive models that match our data require that most of the charges are initially located within their Coulomb attraction radius (see the Supporting Information, Figure S9). This means that most electrons and polarons are spatially located very close to one another and charge separation suffers from their mutual Coulomb attraction. Other charge pairs progressively diffuse away from each other and escape their Coulomb attraction. In particular, the TA measurements show that the yield of electrons decreases from 82 ± 5% at initial times to 24 ± 3% after 1 ps, 10 ± 2% after 10 ps, and 4.5 ± 1% after 500 ps. It is important to point out here that these yield values do not depend on the assumptions made in the diffusion limited recombination model. As noted above, the yield of electrons at 75 fs is referred to as the charge transfer yield or exciton dissociation efficiency and is $\eta_{CT} \sim 82 \pm 5\%$. The fraction of these dissociated excitons that remains after 1 ps (i.e., after the fast recombination) is called charge separation efficiency: $\eta_{sep} \sim (24 \pm 3\%)/(82 \pm 5\%) = 29.5 \pm 4.5\%$.

7. Comparison of Yields Obtained from the Transient Absorption Measurements to Solar Cell Performance. These yields for electron density formation and decay obtained by TA experiments can be compared to the internal quantum efficiency at 800 nm (where IQE is equal to the EQE divided by the fraction of incident photons absorbed in the solar cell). While TA reports on the exciton dissociation efficiency and recombination, the IQE also probes the charge transport and collection efficiencies and therefore should logically be smaller than the TA transfer yield. Let us consider a solar cell with an active layer identical to the hybrid film studied by TA spectroscopy (ITO/PEDOT:PSS/PCPDTBT:CdSe(tBT)/ZnO/Al). It possesses an EQE at 800 nm of 3.7%. For a 2-pass absorption process, the fraction of absorbed photons in a similar active layer deposited on quartz is $\eta_{abs} \sim 17.5\%$ (equal to $2 \times (1 - \%T)$, where $\%T$ is the transmission of the film at 800 nm), resulting in an IQE value at 800 nm of approximately 20%. This suggests that around 80% of the charge carriers remaining at 1 ps (i.e., after the fast recombination time range) are extracted and yield electrical current in a solar cell device under the influence of the electric field induced by the difference in the electrode work functions. Altogether, we have quantified the efficiencies of the following steps in our materials for 800 nm illumination. The external quantum efficiency can be written as $EQE = \eta_{abs} \times \eta_{CT} \times \eta_{sep} \times \eta_{coll}$ with $\eta_{abs} \sim 17.5\%$ the light absorption efficiency (2-pass absorption), $\eta_{CT} \sim 82 \pm 5\%$ the exciton dissociation efficiency (from TA), and $\eta_{sep} \sim 29.5 \pm 4.5\%$ the charge separation efficiency (from TA), so that $\eta_{coll} \sim 80 \pm 20\%$ the charge collection efficiency. The absorption and charge separation efficiencies are here the limiting process in our hybrid solar cell. It is important to mention that the fraction of absorbed photons in a solar cell configuration comprising electrodes and transport layers (rather than on quartz) will be different from the one cited above.[54,55] In effect, it has been shown that the multiple reflections at the various interfaces of the solar cell stack can result in a redistribution of the optical electric field in the active layer, thereby modifying its absorption efficiency. We are currently investigating the magnitude of this effect in our solar cells, and our preliminary results suggest than the fraction of absorbed photons by the active layer in a solar cell configuration is 24% at 800 nm. This results in a charge collection efficiency $\eta_{coll} \sim 66 \pm 14\%$.

To conclude, our study identifies fast geminate recombination as a major source of the carrier loss by direct measurement and, therefore, points to where hybrid blends can be improved. One way to increase the electron–hole initial separation could be to use anisotropic nanostructures.[2,21] With this in mind, our future work will also focus on studying full solar cell devices under operating conditions to further investigate the loss mechanisms in third generation hybrid solar cells in a quantitative fashion.

IV. CONCLUSIONS

We have characterized an efficient hybrid BHJ composed of PCPDTBT and 4.5-nm CdSe QDs capped with *tert*-butylthiol by ultrafast TA spectroscopy. After selective excitation of the low band gap polymer, a clear spectroscopic signature for ultrafast electron transfer to the CdSe(tBT) QDs is observed. The amplitude of this spectral band gives a photon-to-electron transfer yield of 82 ± 5% at initial times (75 fs), while its spectral position identifies the QD energy level filled ($1S_e$) by charge transfer. From the decay of the electron population, we argue that charge pairs are generated in close proximity to each other, which results in strong, unfavorable geminate recombination. This suggests that this is the major loss mechanism for the hybrid blend tested here. Finally, the electron coupling between the PCPDTBT polymer chains and the CdSe(tBT) QDs is found to be $J \gtrsim 17$ meV from the measured lower bound for the forward electron transfer rate, $k \gtrsim 1.5 \times 10^{13}$ s^{-1}.

Recently, it was shown for BHJ containing donor–acceptor polymers blended with PCBM that higher energy excitation led to higher CT rates.[30,56,57] In the case of hybrids, because the electronic coupling probed for low energy excitons (as here with the 800 nm pump) is already very good, we think that

higher energy excitons would open new transfer pathways to other CdSe excited electronic levels rather than increase the rate of electron transfer from the PCPDTBT S_1 exciton to the CdSe(tBT) QDs $1S_e$ level. This variety of transfer pathways could result in a higher global yield of charge transfer. This scenario will be tested in a subsequent study by using various excitation wavelengths in the transient absorption experiment and by comparing the EQE of the solar cell to the absorbance of the active layer in a solar cell configuration. Further studies will also focus on elucidating the impact of the polymer structure, nanocrystal morphology, and ligand chemistry on the electron transfer yield under solar cell operating conditions.

■ ASSOCIATED CONTENT

Supporting Information

Detailed experimental procedures and complementary experimental characterizations; thin film absorbance; *I*−*V* curve of the hybrid solar cell; transient absorption experimental details; statistical analysis to extract most likely bleach decays; and details of the diffusion model for the carrier pair formed inside the Coulomb potential. This material is available free of charge via the Internet at http://pubs.acs.org.

■ AUTHOR INFORMATION

Corresponding Authors

stephen.bradforth@usc.edu
brutchey@usc.edu

Notes

The authors declare no competing financial interest.

■ ACKNOWLEDGMENTS

This work was supported as part of the Center for Energy Nanoscience, an Energy Frontier Research Center funded by the U.S. Department of Energy, Office of Science, Office of Basic Energy Sciences under Award Number DE-SC0001013. R.L.B. also acknowledges the Research Corporation for Science Advancement for a Cottrell Scholar Award. The authors would like to thank Dr. Sean T. Roberts, Saptaparna Das, and Jose Araujo for their assistance.

■ REFERENCES

(1) Zhou, R.; Stadler, R.; Xie, D.; Cao, W.; Zheng, Y.; Yang, Y.; Plaisant, M.; Holloway, P. H.; Schanze, K. S.; Reynolds, J. R.; Xue, J. *ACS Nano* **2013**, *7*, 4846−4854.
(2) Greaney, M. J.; Araujo, J.; Burkhart, B.; Thompson, B. C.; Brutchey, R. L. *Chem. Commun.* **2013**, *49*, 8602−8604.
(3) Reiss, P.; Couderc, E.; De Girolamo, J.; Pron, A. *Nanoscale* **2011**, *3*, 446−489.
(4) Greaney, M. J.; Das, S.; Webber, D. H.; Bradforth, S. E.; Brutchey, R. L. *ACS Nano* **2012**, *6*, 4222−4230.
(5) Clarke, T. M.; Durrant, J. R. *Chem. Rev.* **2010**, *110*, 6736−6767.
(6) Piliego, C.; Loi, M. A. *J. Mater. Chem.* **2012**, *22*, 4141−4150.
(7) Deibel, C.; Strobel, T.; Dyankonov, V. *Adv. Mater.* **2010**, *22*, 4097−4111.
(8) Witt, F.; Kruszynska, M.; Borchert, H.; Parisi, J. *J. Phys. Chem. Lett.* **2010**, *1*, 2999−3003.
(9) Grancini, G.; Biasiucci, M.; Mastria, R.; Scotognella, F.; Tassone, F.; Polli, D.; Gigli, G.; Lanzani, G. *J. Phys. Chem. Lett.* **2012**, *3*, 517−523.
(10) Bensal, N.; Reynolds, L. X.; MacLachlan, A.; Lutz, T.; Ashraf, R. S.; Zhang, W.; Nielsen, C. B.; McCulloch, I.; Rebois, D. G.; Kirchhartz, T.; Hill, M. S.; Molloy, K. C.; Nelson, J.; Haque, S. A. *Sci. Rep.* **2013**, *3*, 1531.
(11) Greenham, N. C.; Peng, X.; Alivisatos, A. P. *Phys. Rev. B* **1996**, *54*, 17628−17637.
(12) ten Cate, S.; Schins, J. M.; Siebbeles, L. D. A. *ACS Nano* **2012**, *6*, 8983−8988.
(13) Piris, J.; Dykstra, T. E.; Bakulin, A. A.; van Loosdrecht, P. H. M.; Knulst, W.; Tuan Trinh, M.; Schins, J. M.; Siebbeles, L. D. A. *J. Phys. Chem. C* **2009**, *113*, 14500−14506.
(14) Herrmann, D.; Niesar, S.; Scharsich, C.; Köhler, A.; Stutzmann, M.; Riedle, E. *J. Am. Chem. Soc.* **2011**, *133*, 18220−18233.
(15) Beek, W. J. E.; Wienk, M. M.; Janssen, R. A. J. *Adv. Mater.* **2004**, *16*, 1009−1013.
(16) Beek, W. J. E.; Wienk, M. M.; Kemerink, M.; Yang, X.; Janssen, R. A. J. *J. Phys. Chem. B* **2005**, *109*, 9505−9516.
(17) Tagliazucchi, M.; Tice, D. B.; Sweeney, C. M.; Morris-Cohen, A. J.; Weiss, E. A. *ACS Nano* **2011**, *5*, 9907−9917.
(18) Heinemann, M. D.; von Maydell, K.; Zutz, F.; Kolny-Olesiak, J.; Borchert, H.; Riedel, I.; Parisi, J. *Adv. Funct. Mater.* **2009**, *19*, 3788−3795.
(19) Itskos, G.; Othonos, A.; Rauch, T.; Tedde, S. F.; Hayden, O.; Kovalenko, M. V.; Heiss, W.; Choulis, S. A. *Adv. Energy Mater.* **2011**, *1*, 802−812.
(20) Bouclé, J.; Chyla, S.; Shaffer, M. S. P.; Durrant, J. R.; Bradley, D. D. C.; Nelson, J. *Adv. Funct. Mater.* **2008**, *18*, 622−633.
(21) Dayal, S.; Kopidakis, N.; Olson, D. C.; Ginley, D. S.; Rumbles, G. *Nano Lett.* **2010**, *10*, 239−242.
(22) Rivera, C. A.; Winter, N.; Harper, R. V.; Benjamin, I.; Bradforth, S. E. *Phys. Chem. Chem. Phys.* **2011**, *13*, 8269−8283.
(23) Roberts, S. T.; Schlenker, C. W.; Barlier, V.; McAnally, R. E.; Zhang, Y.; Mastron, J. N.; Thompson, M. E.; Bradforth, S. E. *J. Phys. Chem. Lett.* **2011**, *2*, 48−54.
(24) Mühlbacher, D.; Scharber, M.; Morana, M.; Zhu, Z.; Waller, D.; Gaudiana, R.; Brabec, C. *Adv. Mater.* **2006**, *18*, 2884−2889.
(25) Webber, D. H.; Brutchey, R. L. *J. Am. Chem. Soc.* **2012**, *134*, 1085−1092.
(26) Norris, D. J.; Bawendi, M. G. *Phys. Rev. B* **1996**, *53*, 16338−16346.
(27) Klimov, V. I.; McBranch, D. W.; Leatherdale, C. A.; Bawendi, M. G. *Phys. Rev. B* **1999**, *60*, 13740−13749.
(28) Couderc, E.; Bruyant, N.; Fiore, A.; Chandezon, F.; Djurado, D.; Reiss, R.; Faure-Vincent, J. *Appl. Phys. Lett.* **2012**, *101*, 133301.
(29) Tsoi, W. C.; Spencer, S. J.; Yang, L.; Ballantyne, A. M.; Nicholson, P. G.; Turnbull, A.; Shard, A. G.; Murphy, C. E.; Bradley, D. D. C.; Nelson, J.; Kim, J.-S. *Macromolecules* **2011**, *44*, 2944−2952.
(30) Grancini, G.; Maiuri, M.; Fazzi, D.; Petrozza, A.; Egelhaaf, H.-J.; Brida, D.; Cerullo, G.; Lanzani, G. *Nat. Mater.* **2013**, *12*, 29−33.
(31) Hwang, I.-W.; Soci, C.; Moses, D.; Zhu, Z.; Waller, D.; Gaudiana, R.; Brabec, C. J.; Heeger, A. J. *Adv. Mater.* **2007**, *19*, 2307−2312.
(32) Yamamoto, S.; Ohkita, H.; Benten, H.; Ito, S. *J. Phys. Chem. C* **2012**, *116*, 14804−14810.
(33) Tautz, R.; Da Como, E.; Limmer, T.; Feldmann, J.; Egelhaaf, H.-J.; von Hauff, E.; Lemaur, V.; Beljonne, D.; Yilmaz, S.; Dumsch, I.; Allard, S.; Scherf, U. *Nat. Commun.* **2012**, *3*, 970.
(34) Wiebeler, C.; Tautz, R.; Feldmann, J.; von Hauff, E.; Da Como, E.; Schumacher, S. *J. Phys. Chem. B* **2013**, *117*, 4454−4460.
(35) Kaake, L. G.; Jasieniak, J. J.; Bakus, B. C.; Welch, G. C.; Moses, D.; Bazan, G. C.; Heeger, A. J. *J. Am. Chem. Soc.* **2012**, *134*, 19828−19838.
(36) Etzold, F.; Howard, I. A.; Forler, N.; Cho, D. M.; Meister, M.; Mangold, H.; Shu, J.; Hansen, M. R.; Muellen, K.; Laquai, F. *J. Am. Chem. Soc.* **2012**, *134*, 10569−10583.
(37) McArthur, E. A.; Morris-Cohen, A. J.; Knowles, K. E.; Weiss, E. A. *J. Phys. Chem. B* **2010**, *114*, 14514−14520.
(38) Knowles, K. E.; McArthur, E. A.; Weiss, E. A. *ACS Nano* **2011**, *5*, 2026−2035.
(39) Colbert, A. E.; Janke, E. M.; Hsieh, S. T.; Subramaniyan, S.; Schlenker, C. W.; Jenekhe, S. A.; Ginger, D. S. *J. Phys. Chem. Lett.* **2013**, *4*, 280−284.

(40) Guyot-Sionnest, P.; Hines, M. A. *Appl. Phys. Lett.* **1998**, *72*, 686−688.
(41) Barbara, P. F.; Meyer, T. J.; Ratner, M. A. *J. Phys. Chem.* **1996**, *100*, 13148−13168.
(42) Coffey, D. C.; Larson, B. W.; Hains, A. W.; Whitaker, J. B.; Kopidakis, N.; Boltalina, O. V.; Strauss, S. H.; Rumbles, G. *J. Phys. Chem. C* **2012**, *116*, 8916−8923.
(43) Watson, D. W.; Meyer, G. J. *Annu. Rev. Phys. Chem.* **2005**, *56*, 119−156.
(44) Carvalho, A.; Martsinovich, N.; Vieira, R.; Troisi, A. *J. Phys. Chem. C* **2013**, *117*, 110−115.
(45) Yang, F.; Forrest, S. R. *ACS Nano* **2008**, *2*, 1022−1032.
(46) Park, S. H.; Roy, A.; Beaupré, S.; Chol, S.; Coates, N.; Moon, J. S.; Moses, D.; Leclerc, M.; Lee, K.; Heeger, A. J. *Nat. Photonics* **2009**, *3*, 297−302.
(47) Press, W. H.; Teukolsky, S. A.; Vetterling, W. T.; Flannery, B. P. *Numerical Recipes in C: the Art of Scientific Computing*; Cambridge University Press: Cambridge, 1988. Press, W. H.; Teukolsky, S. A.; Vetterling, W. T.; Flannery, B. P. *Numerical Recipes in C: the Art of Scientific Computing*; Cambridge University Press: Cambridge, 1988.
(48) This contrasts with the assumption made in the study by ten Cate et al.,[12] where it is assumed that an extra charge yields only half the bleach magnitude compared to the bleach caused by an exciton. While these numbers have not been measured to our knowledge, we use the most conservative assumption for the estimation of the charge transfer yield.
(49) Rice, S. A. *Diffusion-Limited Reactions*; Elsevier: Amsterdam, 1985; Vol. *25*.
(50) Onsager, L. *J. Chem. Phys.* **1934**, *2*, 599−615.
(51) Braun, C. L. *J. Chem. Phys.* **1984**, *80*, 4157−4161.
(52) Groves, C.; Blakesley, J. C.; Greenham, N. C. *Nano Lett.* **2010**, *10*, 1063−1069.
(53) Krissinel', E. B.; Agmon, N. *J. Comput. Chem.* **1996**, *17*, 1085−1098.
(54) Pettersson, L. A. A.; Roman, L. S.; Inganäs, O. *J. Appl. Phys.* **1999**, *86*, 487−496.
(55) Ameri, T.; Dennler, G.; Waldauf, C.; Azimi, H.; Seemann, A.; Forberich, K.; Hauch, J.; Scharber, M.; Hingerl, K.; Brabec, C. J. *Adv. Funct. Mater.* **2010**, *20*, 1592−1598.
(56) Bakulin, A. A.; Rao, A.; Pavelyev, V. G.; van Loosdrecht, P. H. M.; Pshenichnikov, M. S.; Niedzialek, D.; Cornil, J.; Beljonne, D.; Friend, R. H. *Science* **2012**, *335*, 1340−1344.
(57) Tautz, R.; Da Como, E.; Wiebeler, C.; Soavi, G.; Dumsch, I.; Fröhlich, N.; Grancini, G.; Allard, S.; Scherf, U.; Cerullo, G.; Schumacher, S.; Feldmann, J. *J. Am. Chem. Soc.* **2013**, *135*, 4282−4290.